CMS Physics Analysis Summary

Contact: cms-pag-conveners-sus@cern.ch 2025/05/14

Search for Higgsinos in final states with low-momentum lepton-track pairs at 13 TeV

The CMS Collaboration

Abstract

A search for the pair production of Higgsinos in final states with large missing transverse momentum and either two reconstructed muons or a reconstructed lepton (muon or electron) and an isolated track is presented. The analyzed data are proton-proton collisions with an integrated luminosity of 138 fb^{-1} collected by the CMS experiment in proton-proton collisions at $\sqrt{s} = 13$ TeV. The signal scenario considers two neutralino states differing in mass by small values of approximately 0.5–5 GeV, in which the heavier neutralino decays into the lighter neutralino and two same-flavor leptons. The selection focuses on cases in which either the lepton p_{T} or the opening angle between the leptons is smaller than that required by previous searches. Multivariate discriminants are used to enhance the sensitivity by efficiently rejecting backgrounds from SM processes or fake tracks and leptons. The search explores a unique phase space and probes a previously unexplored region in the signal model parameter space. Mass differences between the lightest and next-to-lightest neutralinos are probed as low as 1.5 GeV, assuming a 100 GeV Higgsino, as well as Higgsino masses up to 145 GeV for a mass difference of 4 GeV.

1 Introduction

Physics scenarios beyond the standard model (SM) featuring near-degenerate electroweak doublets or multiplets are well-motivated candidates for dark matter (DM) [1, 2]. For example, in inert doublet [3] and inelastic DM [4, 5] models, the lightest of two or more states–if neutral and stable–may explain the DM relic abundance. Higgsinos in R-parity-conserving supersymmetry (SUSY) [6–14] are also viable DM candidates, not only accounting for DM but also addressing the electroweak hierarchy problem [15, 16]. To resolve these issues, Higgsino masses must typically be of the order of 100 GeV, making them potentially detectable at the LHC. The viable parameter space of these models has been explored and constrained by searches for new physics in the Run 2 (i.e., 2016-2018) data of ATLAS [17] and CMS [18], LEP [19], as well as by DM direct detection experiments [20–22]. Some parameter space remains accessible, particularly in scenarios with more compressed (degenerate) mass spectra.

In the minimal supersymmetric standard model (MSSM), the SM Lagrangian is extended to be invariant under SUSY transformations and includes a second complex scalar doublet. A total of eight Higgs and Higgsino fields before electroweak symmetry breaking give rise to five physical Higgs bosons and four Higgsino mass eigenstates after symmetry breaking. The Higgsinos mix with the superpartners of the W and B bosons (wino and bino) to form chargino ($\widetilde{\chi}_1^{\pm}$) and neutralino ($\widetilde{\chi}_1^0$) states, collectively referred to as electroweakinos. In the limit where the wino and bino mass parameters are much larger than the Higgsino mass parameter, the lightest supersymmetric particle (LSP) emerges as the lightest state $\widetilde{\chi}_1^0$ among the four electroweakino states: $\widetilde{\chi}_1^{\pm}$ and $\widetilde{\chi}_{1,2}^0$. Although small relative to the mass scale, a minimal mass difference of approximately 300 MeV between the chargino and the LSP is required from radiative corrections and cosmological constraints [23].

We present a search for compressed Higgsinos using proton-proton (pp) collision data recorded by CMS at a center-of-mass energy of 13 TeV, targeting events featuring the decay $\widetilde{\chi}_2^0 \to \ell\ell\widetilde{\chi}_1^0$, where ℓ is an electron or muon. The analysis focuses on the scenario where the mass difference $\Delta m^0 = m(\widetilde{\chi}_2^0) - m(\widetilde{\chi}_1^0)$ is twice the value of that between the chargino and the LSP, $\Delta m^{\pm} = m(\widetilde{\chi}_1^{\pm}) - m(\widetilde{\chi}_1^0) = \frac{1}{2}\Delta m^0$, consistent with the limit of large $\tan\beta$. Two processes dominate the total signal production cross section and are illustrated in Fig. 1. In both cases, the decay proceeds via a virtual Z boson, which subsequently decays to a pair of low-momentum (soft) electrons or muons. A branching fraction $\mathcal{B}(\mathrm{Z} \to \mu\mu) = \mathcal{B}(\mathrm{Z} \to \mathrm{ee})$ of 5% is assumed for virtual Z, an approximate upper bound in the MSSM [24]. The chargino decays predominantly to hadrons, most often a single soft pion, via an off-shell W boson [23]. A branching fraction of 100% to this dominant decay mode is assumed. The search targets events with two opposite-charge, same-flavor leptons where the magnitude of the missing transverse momentum ($p_{\mathrm{T}}^{\mathrm{miss}}$) is large.

Previous searches performed at the Large Electron–Positron Collider (LEP) [25–30] exclude charginos with masses up to approximately 90–100 GeV. ATLAS and CMS have previously targeted final states with two reconstructed, isolated leptons [31–33], extending the mass reach to 205 GeV for a mass splitting of 7.5 GeV and to 150 GeV for smaller splittings. However, sensitivity is limited for splittings below 3 GeV, largely because of kinematic and isolation-based selection criteria, particularly those on the lepton transverse momentum (p_{T}) and angular separation, such as $p_{\mathrm{T}} > 3.5$ GeV and $\Delta R(\ell_1, \ell_2) > 3$ [33].

Sensitivity is reduced in phase space between that explored by soft-lepton analyses and that probed by searches targeting charginos with macroscopic lifetimes [34–38]. To improve sensitivity in this region, we analyze events with lepton candidates selected using relaxed kinematic thresholds and identification criteria. Signal regions (SRs) are constructed using boosted deci-

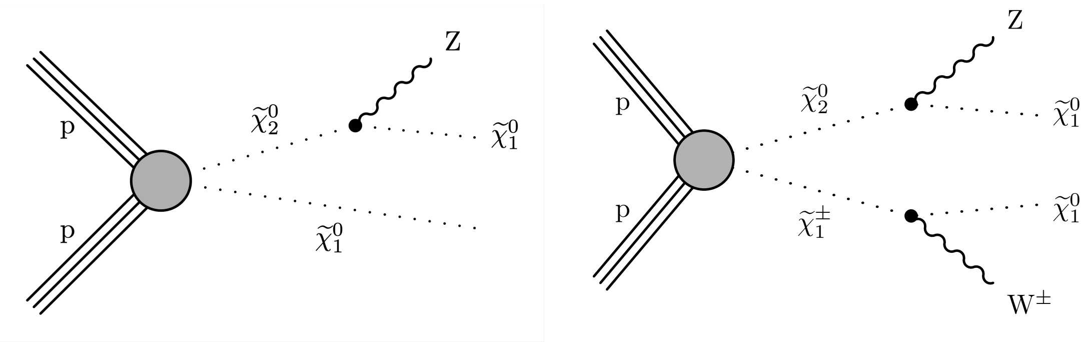

Figure 1: Feynman diagrams illustrating the production and decay of electroweakinos in the Higgsino simplified model, through the $\widetilde{\chi}_2^0\,\widetilde{\chi}_1^0$ (left) and $\widetilde{\chi}_2^0\,\widetilde{\chi}_1^{\pm}$ (right) processes.

sion trees (BDTs) trained to distinguish signal-like events in the target phase space. The SRs are mutually exclusive and statistically disjoint, both with respect to each other and to those used in previous CMS analyses. Three event categories are considered: events with two reconstructed and identified muons; one reconstructed muon and an isolated, exclusive track (t); and one reconstructed electron and an isolated, exclusive track. Here, "exclusive" means the track is not geometrically matched to any identified lepton.

2 CMS detector, reconstruction, and simulation

The CMS apparatus [39, 40] is a multipurpose, nearly hermetic detector, designed to trigger on [41–43] and identify electrons, muons, photons, and (charged and neutral) hadrons [44–46]. A global "particle-flow" (PF) algorithm [47] aims to reconstruct all individual particles in an event, combining information provided by the all-silicon inner tracker and by the crystal electromagnetic and brass-scintillator hadron calorimeters, operating inside a 3.8 T superconducting solenoid, with data from the gas-ionization muon detectors embedded in the flux-return yoke outside the solenoid. The reconstructed particles are used to build jets, and missing transverse momentum [48, 49].

The tracking system, which plays a central role in this analysis, consists of silicon pixel and strip detectors located within the solenoid volume. The inner tracker used during the 2016 data-taking period, referred to as the "Phase-0" tracker, measured charged particles within $|\eta| < 2.5$. An upgraded pixel detector, known as the "Phase-1" tracker, was installed at the beginning of 2017 and used for the 2017 and 2018 data-taking periods. The Phase-1 tracker extended the coverage to $|\eta| < 3.0$. In the barrel region, charged-particle tracks pass through three (four) pixel layers within a radius of 102 (160) mm in the Phase-0 (Phase-1) tracker. The strip tracker provides up to ten additional tracking layers within a radius of 1.2 m. Compared to the Phase-0 tracker, the Phase-1 upgrade improves both tracking and vertex reconstruction performance, and enhances the efficiency of algorithms identifying displaced jets originating from bottom quarks (b jets).

The muon system comprises gas-ionization detectors embedded in the steel flux-return yoke outside the solenoid, enabling muon reconstruction within $|\eta| < 2.4$. It consists of three types of detectors: drift tube chambers in the central region, cathode strip chambers in the forward region, and resistive plate chambers covering both regions. The fine granularity of the forward detectors provides good efficiency for reconstructing low p_{T} muons in the high $|\eta|$ region, which are important for this analysis. In contrast, such muon acceptance is lower in the central region due to the significant curvature of low-p_T charged particles in the magnetic field.

Jets are reconstructed offline from the energy deposits in the calorimeter towers, clustered using the anti-k_T algorithm [50, 51] with a distance parameter of 0.4. In this process, the contribution from each calorimeter tower is assigned a momentum, the absolute value and the direction of which are given by the energy measured in the tower, and the coordinates of the tower. The raw jet energy is obtained from the sum of the tower energies, and the raw jet momentum by the vectorial sum of the tower momenta, which results in a nonzero jet mass. The raw jet energies are then corrected to establish a relative uniform response of the calorimeter in η and a calibrated absolute response in transverse momentum p_T.

Simulated signal events are generated at leading order using the PYTHIA 8.205 generator [52]. To manage computational resources, the detector response for signal events is modeled using the CMS fast simulation framework [53, 54], which yields results generally consistent with those obtained from GEANT4. To improve agreement with GEANT4, a correction of 1% is applied to account for differences in the efficiency of the jet quality requirements [48, 49], and corrections of 5–12% are applied to cover differences in the b tagging efficiency.

Parton showering and hadronization are simulated using the PYTHIA 8.205 generator [52]. For background events, Phase-0 samples use the CUETP8M1 tune [55], while Phase-1 samples use the CP5 tune [56]. Signal samples are generated using the CP2 tune [56]. Samples generated at LO (NLO) with the CUETP8M1 tune use the NNPDF3.0LO (NNPDF3.0NLO) parton distribution functions (PDFs) [57], while those generated with the CP2 or CP5 tune use the NNPDF3.1LO (NNPDF3.1NNLO) PDFs [58].

3 Object and event selection

Signal event candidates for this analysis are recorded using triggers that require the p_T^{miss} to exceed a threshold between 100 and 120 GeV, depending on the instantaneous luminosity of the LHC.

Muons are selected with p_T between 2 and 15 GeV and $|\eta| < 2.4$. Electrons are selected with p_T between 5 and 15 GeV and $|\eta| < 2.5$. Quality criteria are applied to the track fit and the consistency of momentum measurements across subdetectors, aiming to optimize the balance between selection efficiency and the fake rate. Both muons and electrons are required to have an angular separation of $\Delta R > 0.4$ from the leading jet, and to satisfy the jet-based isolation requirement described below.

Jets are selected with $p_T > 15$ GeV and $|\eta| < 5.0$. Two definitions of missing transverse momentum are used: the standard p_T^{miss} and an alternative referred to as hard p_T^{miss}. The hard p_T^{miss} is defined as the magnitude of the vector sum of $\vec{p}_T$ for all reconstructed objects with $p_T > 30$ GeV. Unlike the standard p_T^{miss}, the hard p_T^{miss} is uncorrelated with the isolation variable used to define the signal and control regions, and is more robust against potential mismodeling of pileup.

Tracks are required to have $p_T > 1.9$ GeV and $|\eta| < 2.4$. The relative isolation is defined as the ratio of the scalar sum of p_T of other tracks within a cone of radius 0.3 around the candidate track to the track p_T, and must be less than 0.1. Tracks must have transverse and longitudinal impact parameters with respect to the primary vertex of $|d_{xy}| < 0.02$ cm and $|d_z| < 0.02$ cm, respectively. No selected electron or muon may lie within $\Delta R < 0.01$ of the track. Tracks satisfying these criteria and not geometrically matched to selected leptons are referred to as exclusive tracks.

Dedicated track-picking BDT classifiers are used to identify which track in each signal event corresponds to the lepton from the neutralino decay. Four separate BDTs are trained, corresponding to the two lepton flavors and two detector phases. All classifiers share a common structure of 200 decision trees with a maximum depth of 3, trained using the AdaBoost algorithm and the Gini index as the separation criterion, as implemented in the TMVA package [59].

Training is performed on tracks from a dedicated signal simulation, selected using the same object criteria as the analysis but with slightly loosened requirements: a track $p_{\mathrm{T}} > 1\,\mathrm{GeV}$ and no vetoes based on invariant mass. The preselection described below is applied to the simulated events used in the training sample. A broad range of Higgsino mass parameters, corresponding to $m(\tilde{\chi}_1^{\pm})$, is considered, spanning 100–500 GeV. The training is restricted to models with mass splittings Δm^0 in the range 0.3–4.6 GeV, which corresponds to the targeted analysis phase space. Tracks are labeled as signal if they originate from leptons in the $\tilde{\chi}_2^0 \to \tilde{\chi}_1^0 \ell^+ \ell^-$ decay, as determined by geometrical matching of trajectories, and as background otherwise.

A custom jet-based isolation criterion is defined for leptons using a corrected set of jets. Jets are first selected from among all reconstructed jets with $p_{\mathrm{T}} < 30\,\mathrm{GeV}$. For each such jet, any selected lepton within the jet is vectorially subtracted from the jet momentum. The isolation criterion is binary and determined by two parameters: the lower threshold on the p_{T} of the nearest corrected jet and the upper threshold on the angular separation ΔR between the lepton and that jet. If the lepton does not reside within ΔR of 0.6 of a corrected jet with $p_{\mathrm{T}} > 10$ GeV, it is considered to be isolated.

This isolation variable is uncorrelated with the hard $p_{\mathrm{T}}^{\mathrm{miss}}$ because the soft jets used to define it fall below the p_{T} threshold used in the computation of hard $p_{\mathrm{T}}^{\mathrm{miss}}$. Leptons failing the isolation requirement define a sideband control region, enriched in jet-related background, from which background contributions are estimated as described in Section 4.

3.1 Event selection

The event preselection, common to all analysis categories, consists of the following requirements:

- hard $p_{\mathrm{T}}^{\mathrm{miss}} \geq 220\,\mathrm{GeV}$ and $p_{\mathrm{T}}^{\mathrm{miss}} \geq 140\,\mathrm{GeV}$, to select events efficiently with respect to both signal acceptance and trigger thresholds;
- At least one jet with $p_{\mathrm{T}} \geq 30\,\mathrm{GeV}$ and $|\eta| < 2.4$, to ensure the presence of initial state radiation (ISR);
- $\mathrm{N}_{\mathrm{bjets}} = 0$, to suppress backgrounds from $\mathrm{t\bar{t}}$ production;
- $\min \Delta\phi \left(\text{hard } \vec{p}_{\mathrm{T}}^{\mathrm{miss}}, \vec{j}\right) > 0.4$, to reduce events with mismeasured jets contributing to fake hard $p_{\mathrm{T}}^{\mathrm{miss}}$;
- $N_\ell^{\mathrm{hard}} = 0$, to veto isolated leptons with $p_{\mathrm{T}} \geq 30\,\mathrm{GeV}$, suppressing backgrounds from $\mathrm{W} \to \ell\nu$ decays;
- $0.4 < m_{\ell\ell} < 12\,\mathrm{GeV}$, to remove low-mass resonances and target the compressed mass region of interest.

In the dimuon category, two reconstructed and identified muons are required, and events must satisfy the following criteria:

- $N_\mu = 2$, oppositely charged, satisfying the nominal muon selection;
- $p_{\mathrm{T}}(\mu_2) \leq 3.5\,\mathrm{GeV}$ or $\Delta R(\mu_1, \mu_2) < 0.3$, to ensure no overlap with the search described in Ref. [33];
- $\Delta R(\mu_{1,2}, j_1) > 0.4$, where j_1 is the leading jet;

- $m_{\ell\ell}$ outside the ranges 0.75–0.81 and 3.0–3.2 GeV, to veto ω, ρ^0, and J/ψ resonances;
- Event BDT > 0, to enhance signal purity and reject SM backgrounds.

An event-level classifier is constructed using several observables, including the leading and subleading muon p_T, the ΔR, and $\Delta\eta$ between the two muons, the hard p_T^{miss}, and the differences in azimuthal angle between the hard p_T^{miss} and the muons, as input features. The BDT output distribution is shown in Fig. 2 (left). Six signal region (SR) bins are defined for events with BDT output scores in bins with edges of 0, 0.1, 0.2, 0.3, 0.4, 0.5, and 1, given in order of increasing sensitivity. A single BDT is used for both detector phases.

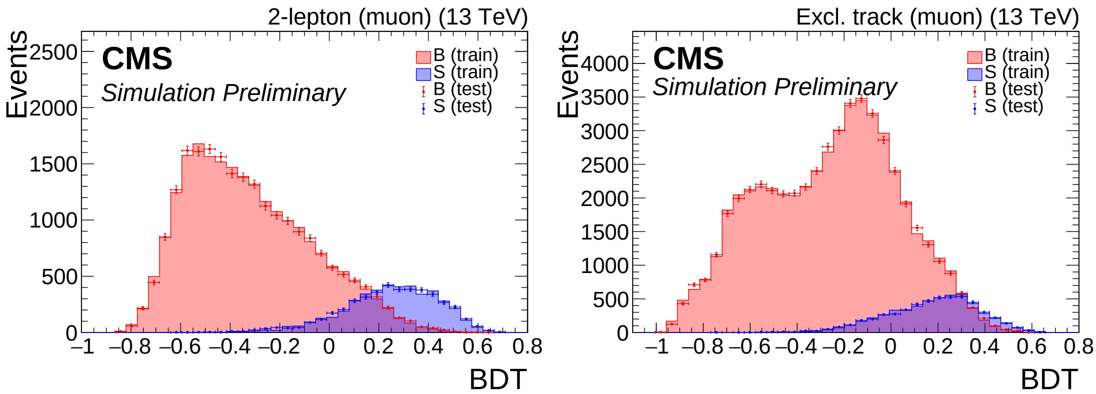

Figure 2: Unweighted distributions of event-level BDT scores for events drawn from the signal and background training samples in the dimuon category (left) and muon+track category (right), based on Phase-1 conditions.

The exclusive track category requires one reconstructed and identified lepton and one exclusive track. The track with the highest score from the track-picking BDT is selected as the recovered lepton candidate. Events in this category must satisfy the preselection and baseline selections, as well as the following additional criteria:

- $N_\ell = 1$, where the lepton passes the analysis muon or electron selection;
- Maximum track BDT score > 0;
- Event BDT score > 0;
- $\Delta R(\ell, j_1) > 0.4$.

Event-level BDT classifiers are used to select signal candidate events in the exclusive track categories while rejecting background events. The output score of each BDT is used to define both the SRs and CRs. Separate BDTs are trained for each lepton flavor and for each detector phase, resulting in a total of five BDTs. The classifiers take as input the ten variables listed in Table 1, ordered by their relative importance as determined by the TMVA algorithm. The most discriminating variable is $\Delta R\,(t, \ell)$, which peaks sharply at low values for signal compared to in-signal background. The invariant mass of the track-lepton system ranks lowest, although one-dimensional distributions indicate that it still provides substantial discriminating power. The BDT captures the mass-related information encoded in the other lepton and track features. 13 SRs are defined in the output of the event BDT for each detector phase and lepton category, with 12 intervals of width 0.05 from 0 to 0.6, and a single SR with BDT > 0.6.

Table 1: Input variables to the BDT used for selecting in-signal tracks in the exclusive track category, ranked by their importance as determined by the TMVA algorithm.

Rank	Variable
1	$\Delta R\,(t,\ell)$
2	$\lvert\Delta\eta\,(t,\ell)\rvert$
3	$p_{\mathrm{T}}(\ell)$
4	$\lvert\Delta\phi\,(t,\text{hard }\vec{p}_{\mathrm{T}}^{\text{miss}})\rvert$
5	$\lvert\Delta\eta\,(t,j_1)\rvert$
6	$\lvert\Delta\phi\,(t,\ell)\rvert$
7	$\lvert\eta\,(t)\rvert$
8	$\lvert\eta\,(\ell)\rvert$
9	$\Delta R\,(\ell,j_1)$
10	$m_{t\ell}$

4 Backgrounds

The most significant backgrounds consist of events with leptons originating either from jets or from decays of electroweak bosons, primarily arising from $\mathrm{W}+\text{jets}\to\ell\nu+\text{jets}$ and $\mathrm{Z}+\text{jets}\to\nu\nu+\text{jets}$ processes. In both cases, at least one of the leptons is nonprompt and originates from jet activity. These backgrounds are grouped into two main categories, and a dedicated method is developed to estimate the contribution from each.

4.1 Background in dimuon category

The dominant background in the dimuon category arises from lepton-track pairs produced in association with jets, primarily from leptons originating in the electroweak decays of hadrons. This *jetty* background is estimated using an isolation sideband control region (CR), defined by inverting the jet-based isolation criterion on the leptons. This region is used to extract a template of the BDT score distribution that is consistent with the shape of the jetty background in the SR. Although most leptons are produced within the cores of jets, the distribution of angular distance between the lepton and the jet exhibits a slowly falling tail that extends into the SR. A second CR, defined by the sideband of the event-level BDT score (BDT <0), is used to normalize the shape, accounting for differences in the jetty background production rate between the isolation sideband and main band. The SR is defined by requiring BDT >0 in the isolation main band. The predicted jetty background in the SR is given by:

$$\hat{\mathrm{N}}^{\mathrm{SR}}_{\mathrm{jetty}}(x)=\frac{\mathrm{N}^{\text{norm CR}}_{\text{main band}}}{\mathrm{N}^{\text{norm CR}}_{\text{sideband}}}\cdot\mathrm{N}^{\mathrm{SR}}_{\text{sideband}}(x),\qquad(1)$$

where x is the binned BDT output. The ratio of yields in the normalization regions is referred to as the transfer factor, $\hat{\mathrm{TF}}_{\mathrm{jetty}}$. The corresponding values are listed in Table 2.

A small contribution to the dimuon category arises from prompt, isolated leptons originating from the $\mathrm{Z}/\gamma^*\to\tau^-\tau^+$ process. This background is estimated using simulated event samples corrected with normalization factors derived in a data CR enriched in Z/γ^* events. The CR selects events with two analysis leptons and requires the observable $m_{\tau\tau}$ to lie within a window of 40–130 GeV, consistent with the Z boson mass. The $m_{\tau\tau}$ observable is based on the *collinear approximation*, first described in Ref. [60] and employed in previous analyses, e.g., Refs. [61, 62]. In this approximation, it is assumed that each τ from Z/γ^* is sufficiently boosted such that its decay products are collinear, and that the only source of missing transverse momentum is the neutrinos from the τ decays. The visible muon momenta, together with $p_{\mathrm{T}}^{\text{miss}}$ and the known τ mass, are used to reconstruct the τ four-vectors and calculate their invariant mass. Contamination from other backgrounds is subtracted by first predicting the jetty background using the method described above and removing those yields from the data in the dedicated $\tau\tau$ CR. The ratio of data to simulation in this region is used to extract the correction factors, denoted as $\hat{\mathrm{TF}}_{\tau\tau}$, which are reported in Table 2.

Table 2: Transfer factors and their associated statistical and total relative uncertainties, used to extrapolate background predictions from control regions to the signal region.

Method	Flavor	Phase	$\hat{\mathrm{TF}}$	Stat. uncertainty	Rel. uncertainty
Jetty	Muon	0	0.73	0.14	19%
Jetty	Muon	1	0.62	0.06	9%
Exclusive track	Muon	0	1.11	0.04	4%
Exclusive track	Muon	1	1.07	0.02	2%
Exclusive track	Electron	0	1.04	0.05	5%
Exclusive track	Electron	1	1.05	0.03	3%
$\tau\tau$	Muon	0	1.18	0.45	38%
$\tau\tau$	Muon	1	0.29	0.26	90%

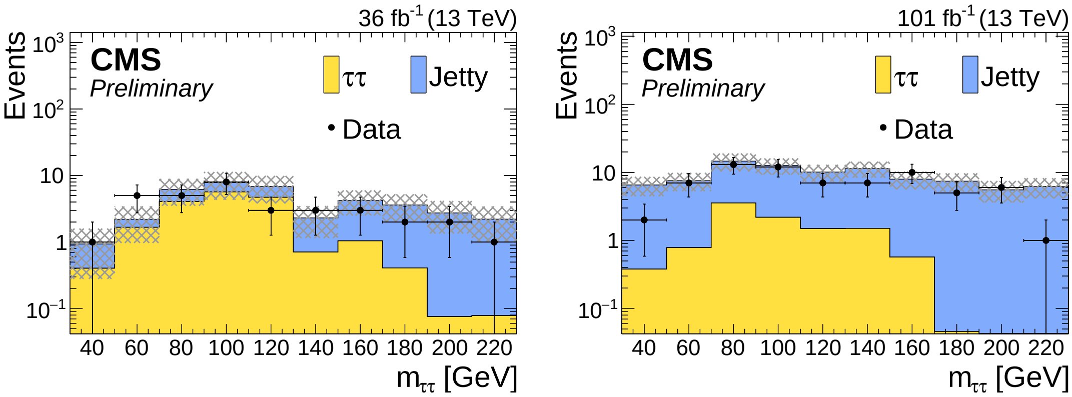

Figure 3: Distributions of the reconstructed ditau invariant mass ($m_{\tau\tau}$) in the BDT sideband control region, shown for Phase-0 (left) and Phase-1 (right). The non-$\tau\tau$ background is estimated using the data-driven jetty background method described in the text.

4.2 Background in exclusive track category

While the nominal selection requires tracks to have opposite charge to the identified lepton, background events featuring same-charge tracks are otherwise kinematically similar for the overwhelming majority of cases. Backgrounds involving isolated leptons from the prompt interaction are found to contribute negligibly to the signal region. Therefore, the background in the SRs of the exclusive track category is estimated using the same-charge CR, defined by inverting the opposite-charge requirement while applying the full analysis selection. The distribution in the same-charge data CR is adjusted with a small normalization correction derived using events with BDT < 0 to match the count in the opposite-sign region. The method is validated through closure tests performed in simulation, comparing the prediction from the data-driven method to the expected result obtained directly from simulation. The resulting normalization factors are $\hat{\mathrm{TF}}_{\text{q-sym}}$ and are reported in Table 2.

4.3 Systematic uncertainty

Systematic uncertainty in the background prediction is assessed based on discrepancies between observed and predicted event counts in control regions (CRs), as well as from validation studies performed using simulation. Uncertainty values range from 8-22% of the estimated yields, increasing with the value of the event classifier. Several sources of uncertainty affecting the signal yield are also identified and estimated, including uncertainty in the modeling of the jet energy response, the p_{T} spectrum of ISR, the efficiency of lepton and b-tagged jet reconstruction, identification, and selection, as well as the integrated luminosity, trigger efficiency, and pileup profile. These uncertainties amount to a total of 5–20% in the signal regions (SRs) and are incorporated into a maximum likelihood fit. Each source of systematic uncertainty is modeled with a log-normal prior, with a corresponding nuisance parameter that modifies the predicted rate of a given process via a multiplicative factor. The width of each log-normal distribution reflects the relative variation in the predicted yield under a one-standard-deviation (σ) shift of the associated uncertainty. Statistical uncertainty is incorporated using gamma-distributed nuisance parameters.

5 Results and interpretation

The results of the analysis are shown in Fig. 4 for the dimuon category and in Fig. 5 for the lepton + exclusive track categories. No significant deviation from the standard model expectation is observed, and the background model provides a good description of the data. A small excess is observed in the most sensitive signal region, more pronounced in the Phase-1 dataset, corresponding to a local significance of approximately 3 standard deviations in Phase-1 and 2.5 standard deviations when combining both datasets.

The results are interpreted in the context of the compressed Higgsino simplified model introduced in Section 1, using a maximum likelihood fit. In this model, the LSP is predominantly Higgsino-like, implying that the Higgsino mass parameter is much smaller than the magnitudes of the bino and wino mass parameters. Both the expected and observed limits are derived using the asymptotic approximation in a maximum likelihood framework. Observed and expected counts are incorporated into the likelihood for all signal regions, corresponding to bins in the results histograms with BDT>0. The $\mathrm{CL_s}$ method [63, 64] is employed to compute exclusion limits at the 95% confidence level.

The exclusion limits are presented in the plane of $\Delta m^{\pm}$ and $m(\tilde{\chi}_1^{\pm})$ in Fig. 6. As discussed in Section 1, the mass splitting between the neutralinos satisfies $\Delta m^0 = 2\Delta m^{\pm}$, consistent with scenarios of large $\tan\beta$. The region enclosed by the exclusion contours is excluded at 95% confidence level, while the color scale indicates the corresponding upper limits on the signal cross section. The green curve represents the minimum allowed value of $\Delta m^{\pm}$ from theoretical calculations that include radiative corrections, following the treatment in Ref. [23]. The sensitivity peaks around $\Delta m^{\pm} \approx 2\,\mathrm{GeV}$, where the analysis excludes charginos up to masses of about 145 GeV, with the observed exclusion reaching up to approximately 115 GeV. Figure 7 provides a comparison of the limits with recent searches targeting the comparessed regime using other final states and complimentary methods.

6 Summary

A search for Higgsino pair production in compressed mass spectra scenarios is performed using low-momentum lepton-track pairs in proton-proton collisions at $\sqrt{s} = 13\,\mathrm{TeV}$, based on a data sample corresponding to an integrated luminosity of $137\,\mathrm{fb}^{-1}$ [68–71] collected with the CMS detector. The results are interpreted in a simplified model featuring a dark matter candidate neutralino that is nearly mass-degenerate with a slightly heavier neutralino and two charginos. The search targets a region of parameter space where sensitivity was limited in pre-

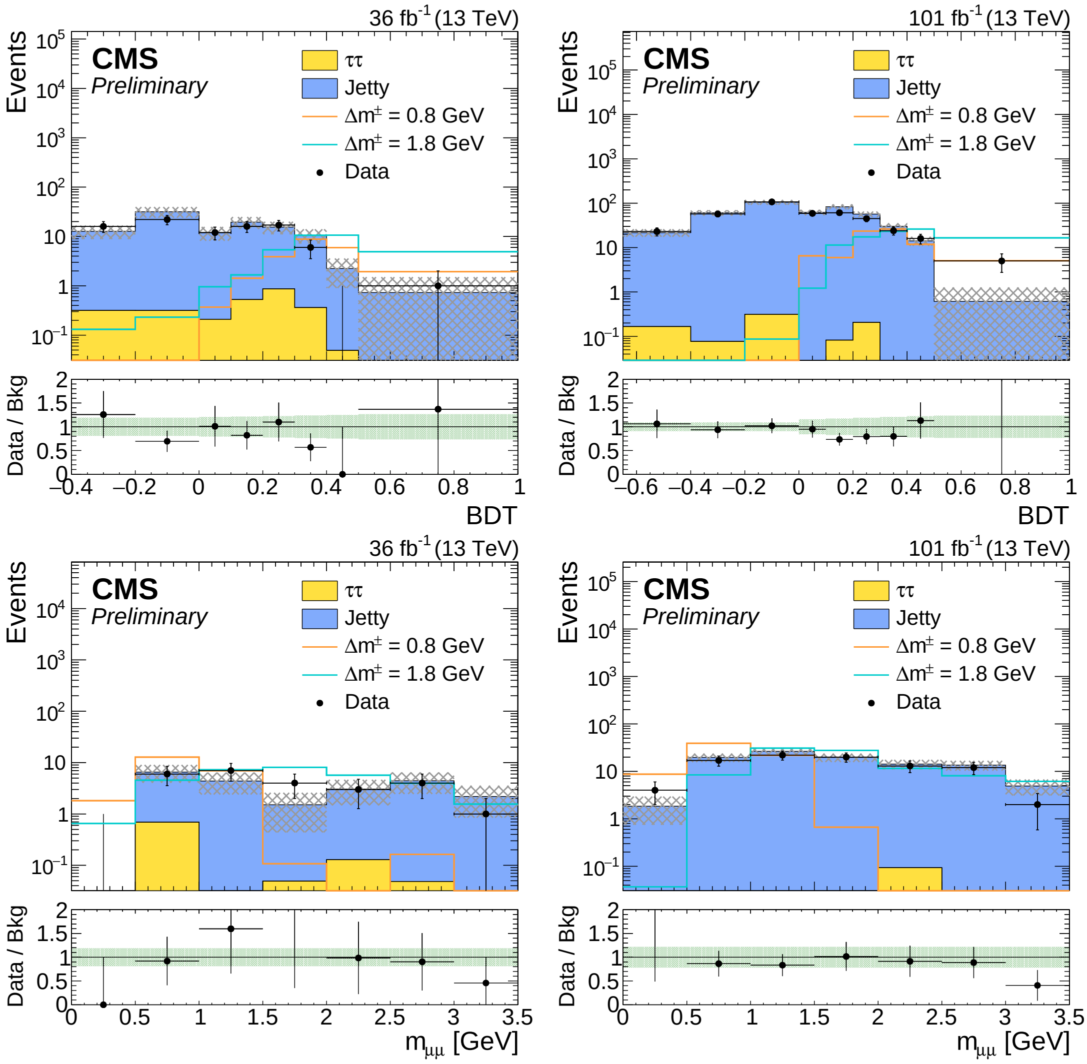

Figure 4: Prefit expected and observed distributions of the event BDT output score in the signal regions for the dimuon category (top) and the dimuon invariant mass in the signal region for events with event classifier scores greater than 0.1 (bottom), shown separately for Phase-0 (left) and Phase-1 (right). The gray hatching shows the statistical uncertainty in the background prediction, while the green band indicates the relative systematic uncertainty in the predicted background. The vertical black bars represent the total uncertainty, including both statistical and systematic components. Two example signal scenarios are also shown as colored lines.

vious analyses. This region, characterized by low-mass Higgsinos, is of particular theoretical interest because of its relevance for naturalness and fine-tuning arguments, offering possible resolutions to both the Large and Small Hierarchy problems. The observed yields are statistically consistent with the background-only hypothesis, though a modest excess is observed in the most sensitive signal regions, more pronounced in Phase-1 than in Phase-0. The local significance of the excess reaches approximately 3 standard deviations. These results place additional constraints on natural supersymmetry and other models predicting electroweak multiplet dark matter.

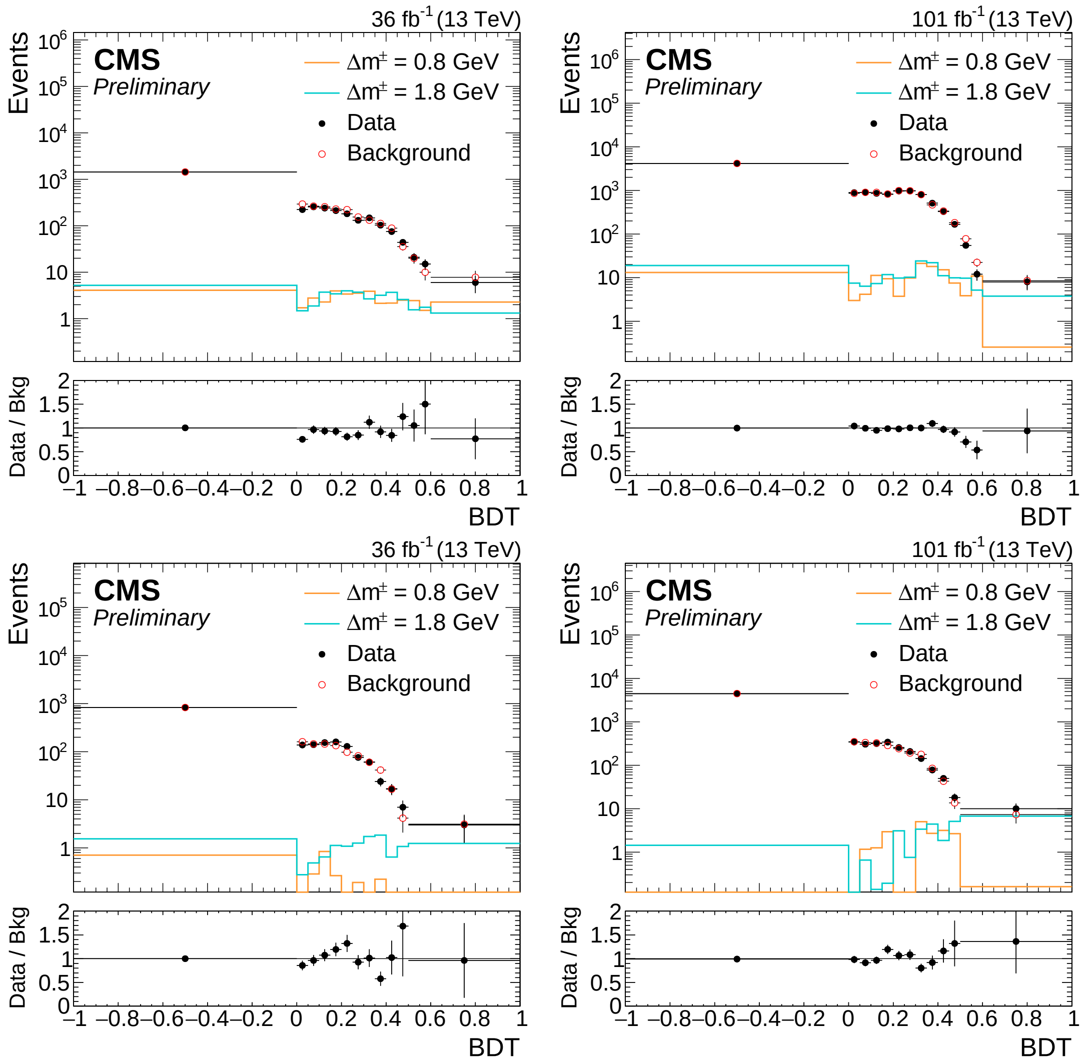

Figure 5: Prefit expected and observed distributions of the event BDT output score in the signal regions for the muon + exclusive track category (top), and the electron + exclusive track category (bottom), shown separately for Phase-0 (left) and Phase-1 (right). The vertical black bars represent the total uncertainty, including both statistical and systematic components. Example signal benchmark scenarios are also shown as colored lines.

References

[1] F. Zwicky, "On the masses of nebulae and of clusters of nebulae", *Astrophys. J.* **86** (1937) 217, doi:10.1086/143864.

[2] V. C. Rubin and W. K. Ford, Jr., "Rotation of the Andromeda nebula from a spectroscopic survey of emission regions", *Astrophys. J.* **159** (1970) 379, doi:10.1086/150317.

[3] L. Lopez Honorez, E. Nezri, J. F. Oliver, and M. H. G. Tytgat, "The Inert Doublet Model: An Archetype for Dark Matter", *JCAP* **02** (2007) 028, doi:10.1088/1475-7516/2007/02/028, arXiv:hep-ph/0612275.

[4] D. Tucker-Smith and N. Weiner, "Inelastic dark matter", *Phys. Rev. D* **64** (2001) 043502, doi:10.1103/PhysRevD.64.043502, arXiv:hep-ph/0101138.

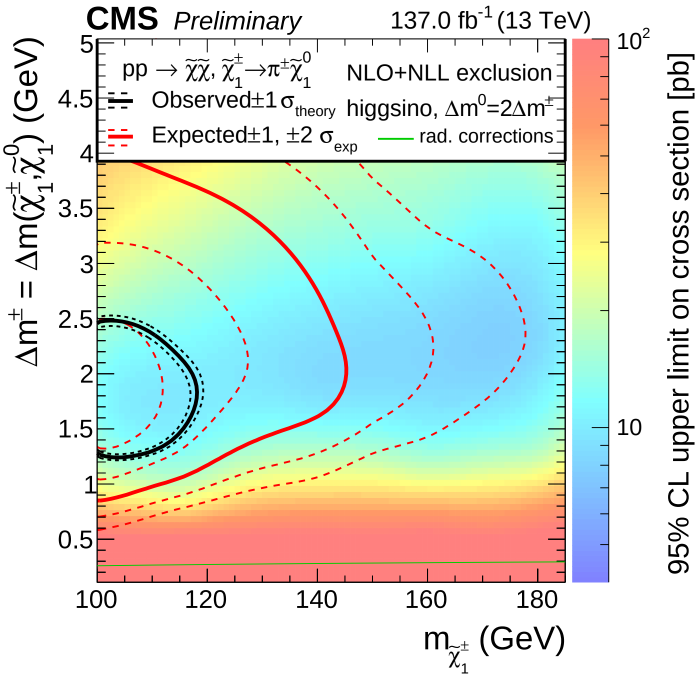

Figure 6: The 95% confidence level (CL) upper limits on the fully-degenerate Higgsino production cross section, calculated at NLO+NLL precision [65, 66], are shown in color in the plane of $\Delta m^{\pm}$ versus the chargino mass. All relevant production modes are simulated at leading order, and the Z^* boson is set to decay into either two electrons or two muons with a branching fraction of 5%. The expected (red) and observed (black) exclusion contours are shown assuming the theoretical cross section. Dashed red lines indicate the expected limits with ± 1 and $\pm 2\ \sigma$) experimental uncertainty. Dashed black lines indicate the observed limit when varying the theoretical cross section by its uncertainty. The green line represents the minimum $\Delta m^{\pm}$ allowed by the theoretical calculation accounting for radiative corrections, as described in [23].

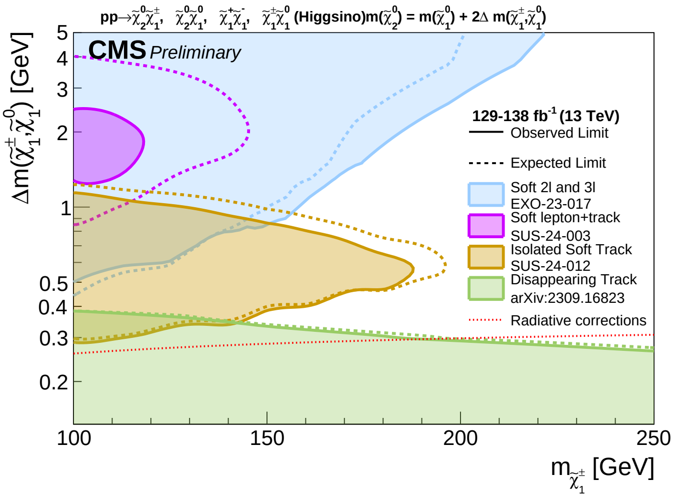

Figure 7: Comparison of limits with analyses featuring final states with disappearing tracks [34], a soft isolated track [38], and soft opposite-sign electron pairs [67].

[5] E. Izaguirre, G. Krnjaic, and B. Shuve, "Discovering Inelastic Thermal-Relic Dark Matter at Colliders", *Phys. Rev. D* **93** (2016) 063523, `doi:10.1103/PhysRevD.93.063523`,

arXiv:1508.03050.

[6] P. Ramond, “Dual theory for free fermions”, *Phys. Rev. D* **3** (1971) 2415, doi:10.1103/PhysRevD.3.2415.

[7] Y. A. Gol’fand and E. P. Likhtman, “Extension of the algebra of Poincaré group generators and violation of P invariance”, *JETP Lett.* **13** (1971) 323, doi:10.1142/9789814542340_0001.

[8] A. Neveu and J. H. Schwarz, “Factorizable dual model of pions”, *Nucl. Phys. B* **31** (1971) 86, doi:10.1016/0550-3213(71)90448-2.

[9] D. V. Volkov and V. P. Akulov, “Possible universal neutrino interaction”, *JETP Lett.* **16** (1972) 438, doi:10.1007/BFb0105270.

[10] J. Wess and B. Zumino, “A Lagrangian model invariant under supergauge transformations”, *Phys. Lett. B* **49** (1974) 52, doi:10.1016/0370-2693(74)90578-4.

[11] J. Wess and B. Zumino, “Supergauge transformations in four dimensions”, *Nucl. Phys. B* **70** (1974) 39, doi:10.1016/0550-3213(74)90355-1.

[12] P. Fayet, “Supergauge invariant extension of the Higgs mechanism and a model for the electron and its neutrino”, *Nucl. Phys. B* **90** (1975) 104, doi:10.1016/0550-3213(75)90636-7.

[13] P. Fayet and S. Ferrara, “Supersymmetry”, *Phys. Rept.* **32** (1977) 249, doi:10.1016/0370-1573(77)90066-7.

[14] H. P. Nilles, “Supersymmetry, supergravity and particle physics”, *Phys. Rep.* **110** (1984) 1, doi:10.1016/0370-1573(84)90008-5.

[15] R. Barbieri and G. F. Giudice, “Upper bounds on supersymmetric particle masses”, *Nuclear Physics B* **306** (1988), no. 1, 63, doi:10.1016/0550-3213(88)90171-X.

[16] B. de Carlos and J. A. Casas, “One-loop analysis of the electroweak breaking in supersymmetric models and the fine-tuning problem”, *Physics Letters B* **309** (jul, 1993) 320, doi:10.1016/0370-2693(93)90940-j.

[17] ATLAS Collaboration, “Statistical Combination of ATLAS Run 2 Searches for Charginos and Neutralinos at the LHC”, *Phys. Rev. Lett.* **133** (2024) 031802, doi:10.1103/PhysRevLett.133.031802, arXiv:2402.08347.

[18] CMS Collaboration, “Combined search for electroweak production of winos, binos, higgsinos, and sleptons in proton-proton collisions at s=13 TeV”, *Phys. Rev. D* **109** (2024) 112001, doi:10.1103/PhysRevD.109.112001, arXiv:2402.01888.

[19] S. Ask, “A Review of the Supersymmetry Searches at LEP”, in *Proceedings of the 38th Rencontres de Moriond: Electroweak Interactions and Unified Theories*, volume 117, p. 185. 2003. arXiv:hep-ex/0305007. doi:10.48550/arXiv.hep-ex/0305007.

[20] LZ Collaboration, “First Dark Matter Search Results from the LUX-ZEPLIN (LZ) Experiment”, *Phys. Rev. Lett.* **131** (2023) 041002, doi:10.1103/PhysRevLett.131.041002, arXiv:2207.03764.

[21] XENON100 Collaboration, "XENON100 Dark Matter Results from a Combination of 477 Live Days", *Phys. Rev. D* **94** (2016) 122001, `doi:10.1103/PhysRevD.94.122001`, `arXiv:1609.06154`.

[22] PandaX Collaboration, "First dark matter search results from the PandaX-I experiment", *Sci. China Phys. Mech. Astron.* **57** (2014) 2024, `doi:10.1007/s11433-014-5598-7`, `arXiv:1408.5114`.

[23] N. Nagata and S. Shirai, "Higgsino dark matter in high-scale supersymmetry", *JHEP* **01** (2015) 029, `doi:10.1007/JHEP01(2015)029`, `arXiv:1410.4549`.

[24] CMS Collaboration, "Phenomenological MSSM interpretation of CMS searches in pp collisions at 13 TeV", technical report, CERN, Geneva, 2024.

[25] ALEPH Collaboration, "Search for charginos nearly mass degenerate with the lightest neutralino in e+ e- collisions at center-of-mass energies up to 209-GeV", *Phys. Lett. B* **533** (2002) 223, `doi:10.1016/S0370-2693(02)01584-8`, `arXiv:hep-ex/0203020`.

[26] A. Heister, S. Schael, and G. Dissertori, "Absolute mass lower limit for the lightest neutralino of the mssm from ee data at s up to 209 gev", *Physics Letters B* **583** (2004) 247, `doi:10.1016/j.physletb.2003.12.066`.

[27] DELPHI Collaboration, "Searches for supersymmetric particles in e+ e- collisions up to 208-GeV and interpretation of the results within the MSSM", *Eur. Phys. J. C* **31** (2003) 421, `doi:10.1140/epjc/s2003-01355-5`, `arXiv:hep-ex/0311019`.

[28] L3collaboration Collaboration, "Search for charginos with a small mass difference to the lightest supersymmetric particle at = 189 GeV", *Physics Letters B* **482** (jun, 2000) 31, `doi:10.1016/s0370-2693(00)00488-3`.

[29] OPAL Collaboration, "Search for anomalous production of dilepton events with missing transverse momentum in e+ e- collisions at s**(1/2) = 183-Gev to 209-GeV", *Eur. Phys. J. C* **32** (2004) 453, `doi:10.1140/epjc/s2003-01466-y`, `arXiv:hep-ex/0309014`.

[30] OPAL Collaboration, "Search for nearly mass degenerate charginos and neutralinos at LEP", *Eur. Phys. J. C* **29** (2003) 479, `doi:10.1140/epjc/s2003-01237-x`, `arXiv:hep-ex/0210043`.

[31] G. Aad and B. Abbott, "Searches for electroweak production of supersymmetric particles with compressed mass spectra in sqrt(s) = 13 tev pp collisions with the ATLAS detector", *Physical Review D* **101** (mar, 2020) `doi:10.1103/physrevd.101.052005`.

[32] ATLAS Collaboration, "Search for chargino–neutralino pair production in final states with three leptons and missing transverse momentum in $\sqrt{s} = 13$ TeV pp collisions with the ATLAS detector", *Eur. Phys. J. C* **81** (2021) 1118, `doi:10.1140/epjc/s10052-021-09749-7`, `arXiv:2106.01676`.

[33] CMS Collaboration, "Search for supersymmetry in final states with two or three soft leptons and missing transverse momentum in proton-proton collisions at $\sqrt{s}$ = 13 TeV", *JHEP* **04** (2022) 091, `doi:10.1007/JHEP04(2022)091`, `arXiv:2111.06296`.

[34] CMS Collaboration, "Search for disappearing tracks in proton-proton collisions at $\sqrt{s} =$ 13 TeV", *Phys. Lett. B* **806** (2020) 135502, `doi:10.1016/j.physletb.2020.135502`, `arXiv:2004.05153`.

[35] ATLAS Collaboration, “Search for long-lived charginos based on a disappearing-track signature using 136 fb^{-1} of pp collisions at $\sqrt{s}$ = 13 TeV with the ATLAS detector”, *Eur. Phys. J. C* **82** (2022) 606, doi:10.1140/epjc/s10052-022-10489-5, arXiv:2201.02472.

[36] CMS Collaboration, “Search for supersymmetry in final states with disappearing tracks in proton-proton collisions at s=13 TeV”, *Phys. Rev. D* **109** (2024) 072007, doi:10.1103/PhysRevD.109.072007, arXiv:2309.16823.

[37] ATLAS Collaboration, “Search for nearly mass-degenerate higgsinos using low-momentum mildly-displaced tracks in pp collisions at $\sqrt{s}$ = 13 TeV with the ATLAS detector”, *Phys. Rev. Lett.* **132** (2024) 221801, doi:10.1103/PhysRevLett.132.221801, arXiv:2401.14046.

[38] CMS Collaboration, “Search for compressed electroweakinos with low-momentum isolated tracks”, technical report, CERN, Geneva, 2025.

[39] CMS Collaboration, “The CMS experiment at the CERN LHC”, *JINST* **3** (2008) S08004, doi:10.1088/1748-0221/3/08/S08004.

[40] CMS Collaboration, “Development of the CMS detector for the CERN LHC Run 3”, *JINST* **19** (2024) P05064, doi:10.1088/1748-0221/19/05/P05064.

[41] CMS Collaboration, “Performance of the CMS Level-1 trigger in proton-proton collisions at $\sqrt{s} = 13\,\text{TeV}$”, *JINST* **15** (2020) P10017, doi:10.1088/1748-0221/15/10/P10017, arXiv:2006.10165.

[42] CMS Collaboration, “The CMS trigger system”, *JINST* **12** (2017) P01020, doi:10.1088/1748-0221/12/01/P01020, arXiv:1609.02366.

[43] CMS Collaboration, “Performance of the CMS high-level trigger during LHC run 2”, *JINST* **19** (2024) P11021, doi:10.1088/1748-0221/19/11/P11021, arXiv:2410.17038.

[44] CMS Collaboration, “Electron and photon reconstruction and identification with the CMS experiment at the CERN LHC”, *JINST* **16** (2021) P05014, doi:10.1088/1748-0221/16/05/P05014, arXiv:2012.06888.

[45] CMS Collaboration, “Performance of the CMS muon detector and muon reconstruction with proton-proton collisions at $\sqrt{s} = 13$ TeV”, *JINST* **13** (2018) P06015, doi:10.1088/1748-0221/13/06/P06015, arXiv:1804.04528.

[46] CMS Collaboration, “Description and performance of track and primary-vertex reconstruction with the CMS tracker”, *JINST* **9** (2014) P10009, doi:10.1088/1748-0221/9/10/P10009, arXiv:1405.6569.

[47] CMS Collaboration, “Particle-flow reconstruction and global event description with the CMS detector”, *JINST* **12** (2017) P10003, doi:10.1088/1748-0221/12/10/P10003, arXiv:1706.04965.

[48] CMS Collaboration, “Jet energy scale and resolution in the CMS experiment in pp collisions at 8 TeV”, *JINST* **12** (2017) P02014, doi:10.1088/1748-0221/12/02/P02014, arXiv:1607.03663.

[49] CMS Collaboration, "Performance of missing transverse momentum reconstruction in proton-proton collisions at $\sqrt{s} = 13$ TeV using the CMS detector", *JINST* **14** (2019) P07004, doi:10.1088/1748-0221/14/07/P07004, arXiv:1903.06078.

[50] M. Cacciari, G. P. Salam, and G. Soyez, "The anti-k_t jet clustering algorithm", *JHEP* **04** (2008) 063, doi:10.1088/1126-6708/2008/04/063, arXiv:0802.1189.

[51] M. Cacciari, G. P. Salam, and G. Soyez, "FastJet user manual", *Eur. Phys. J. C* **72** (2012) 1896, doi:10.1140/epjc/s10052-012-1896-2, arXiv:1111.6097.

[52] T. Sjöstrand et al., "An Introduction to PYTHIA 8.2", *Comput. Phys. Commun.* **191** (2015) 159, doi:10.1016/j.cpc.2015.01.024, arXiv:1410.3012.

[53] S. Abdullin et al., "The fast simulation of the CMS detector at LHC", *J. Phys. Conf. Ser.* **331** (2011) 032049, doi:10.1088/1742-6596/331/3/032049.

[54] A. Giammanco, "The fast simulation of the CMS experiment", *J. Phys. Conf. Ser.* **513** (2014) 022012, doi:10.1088/1742-6596/513/2/022012.

[55] CMS Collaboration, "Event generator tunes obtained from underlying event and multiparton scattering measurements", *Eur. Phys. J. C* **76** (2016) 155, doi:10.1140/epjc/s10052-016-3988-x, arXiv:1512.00815.

[56] CMS Collaboration, "Extraction and validation of a new set of CMS PYTHIA8 tunes from underlying-event measurements", *Eur. Phys. J. C* **80** (2020) 4, doi:10.1140/epjc/s10052-019-7499-4, arXiv:1903.12179.

[57] NNPDF Collaboration, "Parton distributions with QED corrections", *Nucl. Phys. B* **877** (2013) 290, doi:10.1016/j.nuclphysb.2013.10.010, arXiv:1308.0598.

[58] NNPDF Collaboration, "Parton distributions from high-precision collider data", *Eur. Phys. J. C* **77** (2017) 663, doi:10.1140/epjc/s10052-017-5199-5, arXiv:1706.00428.

[59] J. Therhaag, "TMVA Toolkit for multivariate data analysis in ROOT", *PoS* (2010) 510, doi:10.22323/1.120.0510.

[60] R. K. Ellis, I. Hinchliffe, M. Soldate, and J. J. Van Der Bij, "Higgs decay to $\tau^+\tau^-$-a possible signature of intermediate mass higgs bosons at high energy hadron colliders", *Nuclear Physics B* **297** (1988) 221, doi:10.1016/0550-3213(88)90019-3.

[61] ATLAS Collaboration, "Expected Performance of the ATLAS Experiment - Detector, Trigger and Physics", 1, 2009. arXiv:0901.0512. doi:10.48550/arXiv.0901.0512.

[62] CMS Collaboration, "CMS technical design report, volume II: Physics performance", *J. Phys. G* **34** (2007) 995, doi:10.1088/0954-3899/34/6/S01.

[63] T. Junk, "Confidence level computation for combining searches with small statistics", *Nucl. Instrum. Meth. A* **434** (1999) 435, doi:10.1016/S0168-9002(99)00498-2, arXiv:hep-ex/9902006.

[64] A. L. Read, "Presentation of search results: the cls technique", *Journal of Physics G: Nuclear and Particle Physics* **28** (sep, 2002) 2693, doi:10.1088/0954-3899/28/10/313.

[65] B. Fuks, M. Klasen, D. R. Lamprea, and M. Rothering, “Gaugino production in proton-proton collisions at a center-of-mass energy of 8 TeV”, *JHEP* **10** (2012) 081, doi:10.1007/JHEP10(2012)081, arXiv:1207.2159.

[66] B. Fuks, M. Klasen, D. R. Lamprea, and M. Rothering, “Precision predictions for electroweak superpartner production at hadron colliders with RESUMMINO”, *Eur. Phys. J. C* **73** (2013) 2480, doi:10.1140/epjc/s10052-013-2480-0, arXiv:1304.0790.

[67] CMS Collaboration, “Search for new physics with compressed mass spectra in final states with soft leptons and missing transverse energy in proton-proton collisions at $\sqrt{s} = 13$ TeV”, technical report, CERN, Geneva, 2025.

[68] CMS Collaboration, “Precision luminosity measurement in proton-proton collisions at $\sqrt{s} = 13$ TeV in 2015 and 2016 at CMS”, *Eur. Phys. J. C* **81** (2021) 800, doi:10.1140/epjc/s10052-021-09538-2, arXiv:2104.01927.

[69] CMS Collaboration, “CMS luminosity measurement for the 2017 data-taking period at $\sqrt{s}$ = 13 TeV”, CMS Physics Analysis Summary CMS-PAS-LUM-17-004, 2018.

[70] CMS Collaboration, “CMS luminosity measurement for the 2018 data-taking period at $\sqrt{s}$ = 13 TeV”, CMS Physics Analysis Summary CMS-PAS-LUM-18-002, 2019.

[71] A. Giraldi, “Precision luminosity measurement with proton-proton collisions at the CMS experiment in Run 2”, in *Proc. 41st Int. Conf. on High Energy Physics (ICHEP2022)*, p. 638. 2022. arXiv:2208.08214. [PoS(ICHEP2022)638]. doi:10.22323/1.414.0638.